A Finite Element Model for the Computation of the Transfer Impedance of Cable Shields

Ruben Otin[1], Jaco Verpoorte[2], and Harmen Schippers[2]

[1]International Center for Numerical Methods in Engineering (CIMNE), Barcelona, Spain.
E-mail: rotin@cimne.upc.edu

[2]National Aerospace Laboratory (NLR), Amsterdam, the Netherlands.
E-mails: verpoor@nlr.nl, schipiw@nlr.nl.

Abstract - The transfer impedance of a cable shield is a parameter that characterizes its shielding effectiveness. To calculate this parameter we can use analytical or semi-empirical approaches but, in this work, the objective is to adapt a general-purpose finite element formulation. The advantage of a numerical method is that it can be applied to a wider variety of situations where complex geometries and materials may be present. To obtain numerically the transfer impedance we first express it as a function of the electric field and then we compute the field by means of the finite element method. The only input data required in the process are the geometry and the material properties of the shield. To validate our numerical model we apply it to a few cable shields and compare the results of the simulations with analytical models and measurements obtained from the literature.

1 Introduction

The transfer impedance Z_t (also known as surface transfer impedance) characterizes the quality of a cable shield. A lower transfer impedance indicates a good shielding against interfering electromagnetic fields. This concept was initially introduced by Schelkunoff in [1] and it is an intrinsic parameter that represents, independently of environmental factors, the shielding effectiveness of a cable shield. Also, the measurement of Z_t is relatively easy to perform and the experimental setup provides accuracy and repeatability (for a review of measurements methods see for instance [2]).

The knowledge of Z_t is important because it determines the coupling of interference to the wires inside the cable shield. An interference current will be induced in the shield of a cable which is exposed to an electromagnetic

field, either because the cable acts as an antenna or because the (grounded) shield is part of a loop in which an interference voltage is induced. In the latter case an interference current will flow depending on the impedance of the loop. If the transfer impedance is known the common mode voltage between the inner conductors and the shield can be determined. Therefore, with the knowledge of Z_t, we can estimate the effect produced by an external field in the wires inside the cable, or reciprocally, we can also estimate the radiation leaked from inside the cable to the environment.

A number of analytical and empirical approaches have been formulated in the past to determine the transfer impedance of cable shields, specially to the most usual arrangement based on braided metal wires [3–8]. The low and medium frequency behavior of the transfer impedance (DC resistance and skin depth) can be determined quite accurately with these models. However, the behavior of the inductance of the metal braid is very complex. The accuracy of the analytical and empirical models for the higher frequencies in which the inductance plays an important role is sometimes poor. A numerical approach might provide a higher accuracy especially for the high frequency behavior. Also, it can be applied systematically to a wider variety of situations where complex geometries and materials may be present.

The objective of this work is to develop a numerical model for the computation of the transfer impedance of cable shields. This numerical numerical model is based on the finite element method (FEM). In the following sections we explain how to apply a general-purpose finite element formulation to the specific problem of computing Z_t. Firstly, we obtain the electric field using the finite element method. The input data of this process are the geometry and the material properties of the shield. Secondly, we express the transfer impedance as a function of the electric field. This is done re-expressing the definition of Z_t by means of some surface integrals. Finally, we integrate the calculated electric field in these surfaces to obtain Z_t.

The finite element method employed in this work is based on the regularized Maxwell's equations and uses nodal (Lagrangian) elements [9]. This formulation is different from the most extended one based on edge elements and the double-curl Maxwell's equations (see [10,11] and references therein). Although our finite element approach can be more complex to implement, it has the advantage of producing well-conditioned matrices, even at low frequencies, without the need of Lagrange multipliers. On the other hand, our numerical model can be easily adapted to any other FEM formulation. You only need to calculate the electric field with your preferred formulation or a "black-box" commercial software and then perform the surface integrals defined in the following sections.

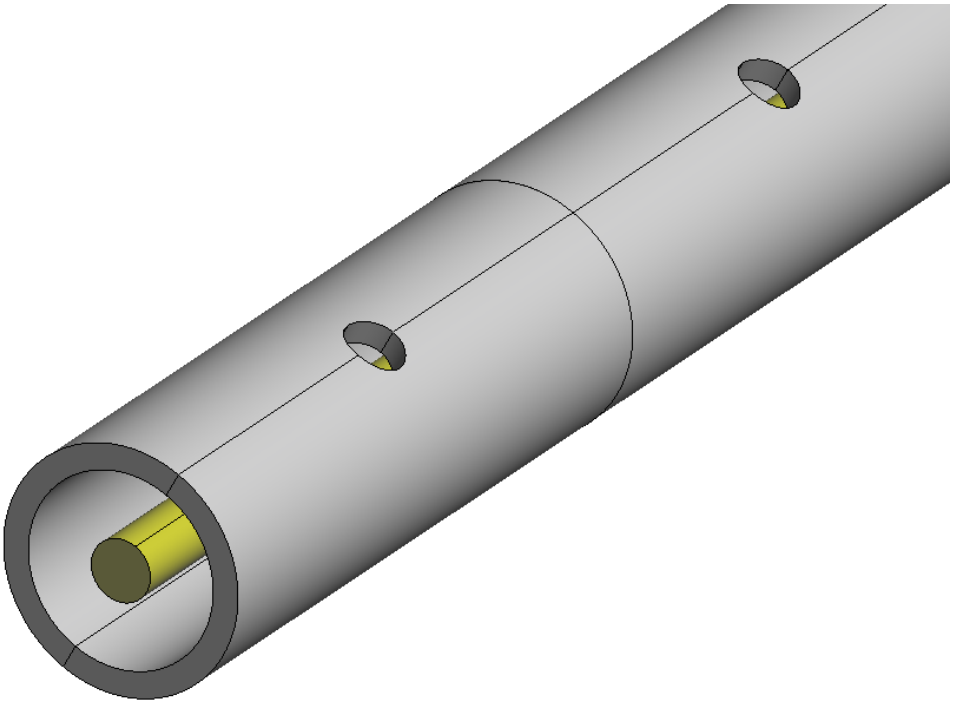

Figure 1: Perforated tube with 22 circular holes per meter. Each hole has a diameter $d_h = 3.175\,\text{mm}$. The thickness of the wall is $T = 1.683\,\text{mm}$. The external diameter of the tube is $D_{ext} = 15.875\,\text{mm}$. The tube is made of brass with an electrical conductivity of $\sigma = 13.32e6\,\text{S/m}$.

To validate our numerical model we calculated the transfer impedance of a few cable shields and compared the results of the simulations with analytical methods and measurements obtained from the literature. The shield configurations selected here for comparing simulations with measurements are perforated tubes. The reason for this selection is that the usual braided wire shields present some uncertainties which can hinder the validation process. This uncertainties are due mainly to the contact impedance between adjacent and porpoising wires or changes in the properties because of aging and handling [12]. The objective of the present paper is to show that our finite element model can give accurate results. It is left for a future work the application of the numerical model to the study of braided wires shields.

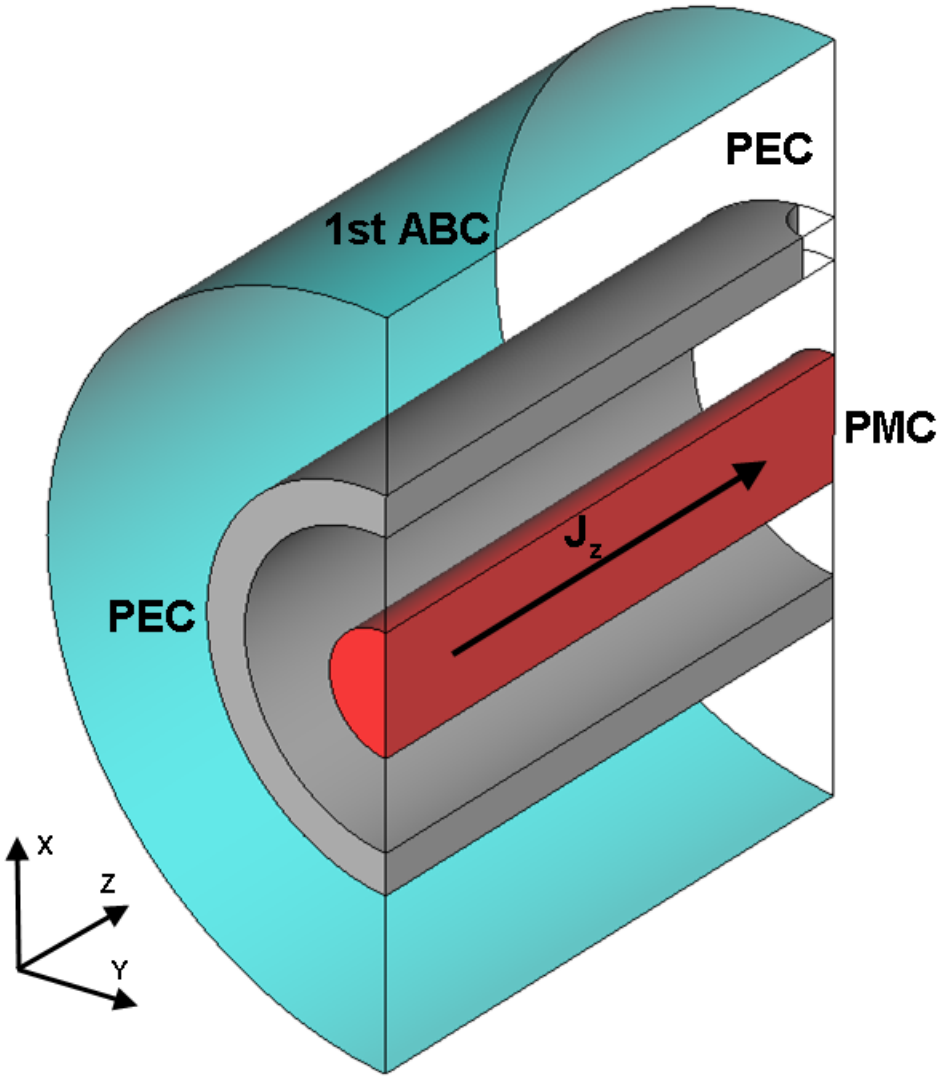

Figure 2: Detail of the geometry of the shield shown in fig. 1. This geometrical set-up was used to compute the electric field with FEM. In the two transversal surfaces is applied a perfect electric conductor boundary condition (PEC). In the longitudinal surface is applied a perfect magnetic boundary condition (PMC). In the exterior curved surface is applied a first order absorbing boundary condition (1st ABC). The problem is driven by a volumetric current density J_z located along the central axis of the shield.

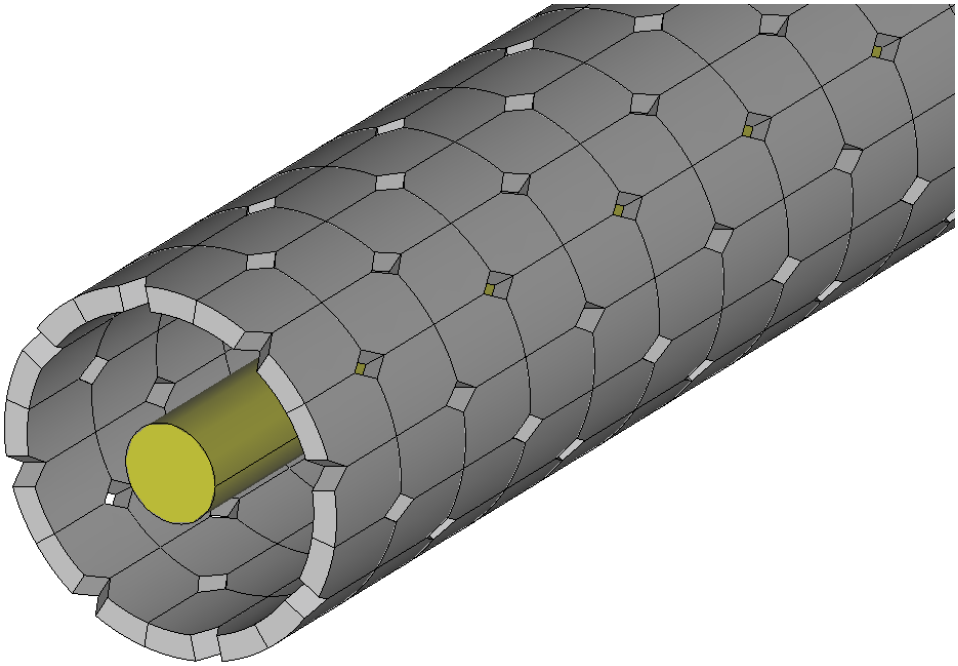

Figure 3: Geometry of the shield of a standard RG 58 coaxial cable tinned (section 4.3). This cable shield was modeled as a perforated tube with rhomboidal holes. The thickness of the shield is $T = 2d$, being d the diameter of the wires of the braid ($d = 0.12\,\mathrm{mm}$). The external diameter of shield is $D_{ext} = 3.5\,\mathrm{mm}$. The braid angle is $\theta = 32.32^{\mathrm{o}}$. The numbers of carriers is $C = 16$ and the number of wires in each carrier is $N = 7$. The electrical conductivity is $\sigma = 32.4e6\,\mathrm{S/m}$, which is the average between the conductivity of copper given in [13] ($\sigma = 56e6\,\mathrm{S/m}$) and the conductivity of tin ($\sigma = 8.8e6\,\mathrm{S/m}$ [14]).

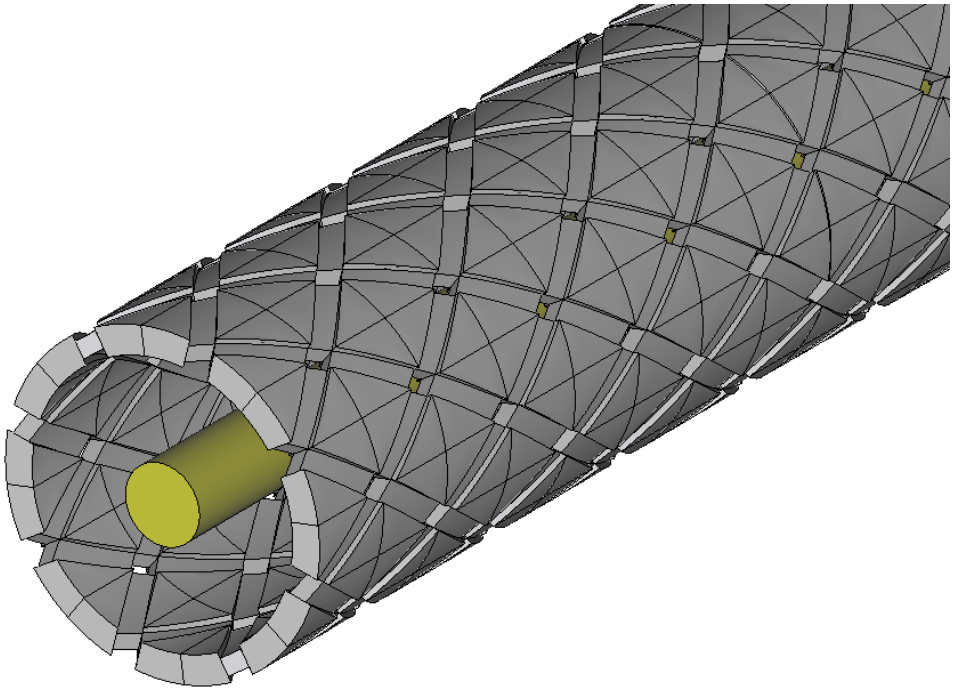

Figure 4: Geometry of the shield of a standard RG 58 coaxial cable tinned (section 4.3). This cable shield was modeled as a perforated tube with rhomboidal holes. In the areas where the carriers of the braid overlap each other the thickness of the shield is $T = 2.5d$ [15], being d the diameter of the wires of the braid ($d = 0.12\,\mathrm{mm}$). In the areas where the carriers of the braid do not overlap each other the thickness of the shield is $T = 1.5d$. The external diameter of shield is $D_{ext} = 3.5\,\mathrm{mm}$. The braid angle is $\theta = 32.32^{\mathrm{o}}$. The numbers of carriers is $C = 16$ and the number of wires in each carrier is $N = 7$. The electrical conductivity is $\sigma = 32.4e6\,\mathrm{S/m}$, which is the average between the conductivity of copper given in [13] ($\sigma = 56e6\,\mathrm{S/m}$) and the conductivity of tin ($\sigma = 8.8e6\,\mathrm{S/m}$ [14]).

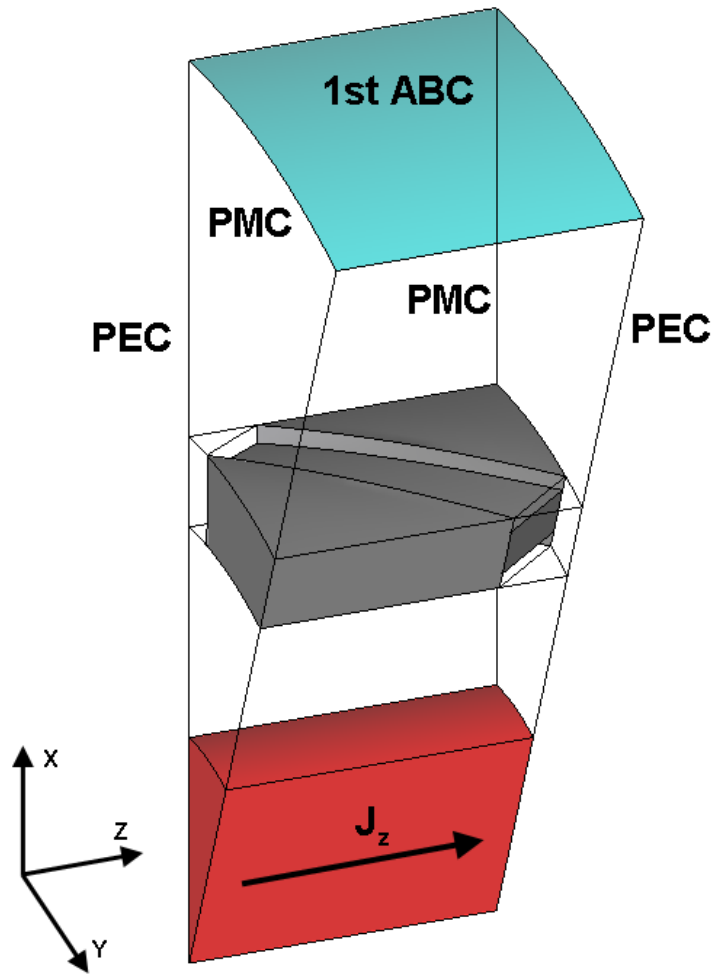

Figure 5: Detail of the geometry of the shield shown in fig. 4. This geometrical set-up was used to compute the electric field with FEM. In the two transversal surfaces is applied a perfect electric conductor boundary condition (PEC). In the two longitudinal surfaces is applied a perfect magnetic boundary condition (PMC). In the upper curved surface is applied a first order absorbing boundary condition (1st ABC). The problem is driven by a volumetric current density J_z located along the central axis of the shield.

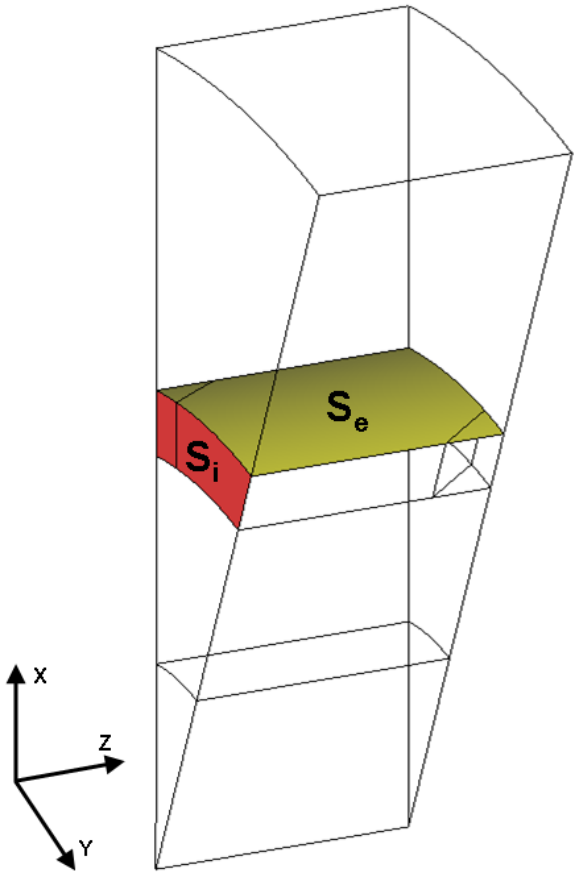

Figure 6: Minimum portion of the shield shown in fig. 3 necessary to compute its transfer impedance. If we know the value of the electric field **E** in the surfaces S_e and S_i we can compute Z_t. We must integrate E_z over S_e to obtain the longitudinal electric field averaged over the outer surface of the shield and $J = \sigma E$ over S_i to obtain a sixteenth of the total induced electric current going through the shield. We have only a sixteenth of the total electric current because S_i is a sixteenth of the whole transversal section of the geometry in fig. 3. Therefore, to calculate the total current, we must multiply by sixteen the value of the integral (3). On the other hand, the integral (2) does not need such a multiplication. Performing the integral (2) over the surface S_e give us the same result as if we performed the integral over the whole outer surface of the shield.

2 Definitions

The transfer impedance Z_t (Ohms/meter) of a cable shield is defined as [1,3]

$$Z_t = \frac{1}{I_0}\frac{\partial V}{\partial z} \tag{1}$$

where I_0 is the current flowing through the shield induced on its outer surface and $\partial V/\partial z$ is the voltage per unit length on the inside of the shield.

Definition (1) can be re-expressed as a function of the electric field by means of the relations

$$\frac{\partial V}{\partial z} = \frac{1}{A_e}\iint_{S_e} E_z \, dS_e \tag{2}$$

and

$$I_0 = \iint_{S_i} \sigma E \, dS_i, \tag{3}$$

where E is the modulus of the electric field, E_z is the modulus of the longitudinal component of the electric field, S_e is the inner surface of the cable shield, S_i is its transversal surface, A_e is the area of S_e and σ is the electrical conductivity of the shield. Equation (2) represents the transversal electric field averaged over the inner surface of the shield and equation (3) represents the induced current going through it.

The transfer impedance can also be defined, by reciprocity, as the ratio between the voltage per unit length on the outer surface of the shield and the current flowing through the shield induced on its inner surface [12]. In this last case, S_e is the outer surface of the cable shield and (2) represents the transversal electric field averaged over its outer surface (see fig. 6).

3 Numerical Model

It is clear from relations (2) and (3) that, in order to obtain Z_t, we need first to compute the electric field. In this section we explain how to do it. First, we give a brief summary of the general finite element formulation used in this work, and next, we show how to adapt this formulation to the specific problem of computing the transfer impedance.

3.1 Finite Element Formulation

In this subsection we give a brief summary of the finite element formulation we utilized to compute the electric field. A more detailed explanation can be found in [9].

In our numerical model we solve the weak form of the regularized Maxwell's wave equation [16], that is, if we define

$$\begin{aligned}&\mathbf{H}\left(\mathbf{curl}, \operatorname{div}; \Omega\right) := \\ &\left\{\mathbf{F} \in \mathbf{L}^2\left(\Omega\right) \mid \nabla \times \mathbf{F} \in \mathbf{L}^2\left(\Omega\right), \nabla \cdot \left(\varepsilon \mathbf{F}\right) \in L^2\left(\Omega\right)\right\},\end{aligned} \tag{4}$$

where $L^2\left(\Omega\right)$ is the space of square integrable functions in the domain Ω and $\mathbf{L}^2\left(\Omega\right)$ the space of vectorial functions with all its components belonging to $L^2\left(\Omega\right)$ then, solving the weak form of the regularized Maxwell's wave equation consists in finding $\mathbf{E} \in \mathbf{H}\left(\mathbf{curl}, \operatorname{div}; \Omega\right)$ such that, $\forall\, \mathbf{F} \in \mathbf{H}\left(\mathbf{curl}, \operatorname{div}; \Omega\right)$ holds

$$\begin{aligned}&\int_\Omega \frac{1}{\mu}\left(\nabla \times \mathbf{E}\right) \cdot \left(\nabla \times \bar{\mathbf{F}}\right) \\ &+ \int_\Omega \frac{1}{\mu\varepsilon\bar{\varepsilon}}\left(\nabla \cdot \left(\varepsilon \mathbf{E}\right)\right) \cdot \left(\nabla \cdot \left(\bar{\varepsilon}\bar{\mathbf{F}}\right)\right) - \omega^2 \int_\Omega \varepsilon\left(\mathbf{E} \cdot \bar{\mathbf{F}}\right) \\ &- \oint_{\partial\Omega} \frac{1}{\mu}\left(\nabla \times \mathbf{E}\right) \cdot \left(\hat{\mathbf{n}} \times \bar{\mathbf{F}}\right) \\ &- \oint_{\partial\Omega} \frac{1}{\mu\varepsilon\bar{\varepsilon}}\left(\nabla \cdot \left(\varepsilon \mathbf{E}\right)\right) \cdot \left(\hat{\mathbf{n}} \cdot \left(\bar{\varepsilon}\bar{\mathbf{F}}\right)\right) = -j\omega \int_\Omega \mathbf{J} \cdot \bar{\mathbf{F}},\end{aligned} \tag{5}$$

where Ω is the problem domain, $\partial\Omega$ is the boundary of Ω, $\hat{\mathbf{n}}$ is the exterior unit normal of the boundary $\partial\Omega$, $\mathbf{E}$ is the electric field, ω is the angular frequency, $\mathbf{J}$ is the current density, μ is the magnetic permeability and ε is the electric permittivity ($\varepsilon = \epsilon - j\sigma/\omega$). The bar over the magnitudes denotes the complex conjugate.

It is shown in [16] that, analytically, solving the *regularized* weak formulation (5) is completely equivalent to solving the *classical* time-harmonic Maxwell's wave equation. However, we must be careful when solving (5) numerically with nodal (Lagrangian) finite elements. If the electric field $\mathbf{E}$ is singular at some point of the domain, the analytical solution obtained from the *classical* Maxwell's equations (the physical solution) can not be approximated with nodal elements and (5), no matter the element size or the polynomial order used in the discretization [17–19].

To avoid this known problem we remove the divergence term of (5) (the first term on the second line) from the elements which are near the points of the domain where the electric field is singular [9]. In our case, these points are the edges and corners of dielectrics or electric conductors and the intersection of several dielectrics or electric conductors [20]. In [9] is shown that for tetrahedral second order nodal elements we need three layers of these special elements around the singularity to obtain good results.

This procedure is a simplification of the weighted regularized Maxwell equation method [21]. In [22, 23] the same strategy is followed for quasi-static problems.

We also consider explicitly the discontinuities of the normal component of the electric field at the interface between different media. At a surface separating two different materials is used the double-node technique given in [24]. For the general case of the intersection of three or more different materials we follow the procedure explained in [9].

This FEM formulation had been implemented in a C++ code called ERMES (*E*lectric *R*egularized *M*axwell *E*quations with *S*ingularities). ERMES had been applied successfully to microwave engineering [25], specific absorbtion rate computations [26, 27] and to the determination of the magnetic pressure and induced eddy currents in electromagnetic sheet metal forming [28]. For geometric modeling, meshing, and visualization of results is used the commercial software GiD [29].

3.2 Finite Element Model for Computing Z_t

In this subsection we explain how to adapt the finite element formulation presented above to the specific problem of computing the transfer impedance. That is to say, we are going to describe the boundary conditions and the sources employed in our numerical model.

The first step to calculate the electric field is to take a portion of an infinitely long cable shield (see fig. 1 and fig. 2 or fig. 4 and fig. 5). Thanks to the special characteristics of our problem we only need to compute the electric field in a portion of the shield. The only requirement to select this portion is that it must have the capacity to generate the whole shield geometry after applying consecutively a mirror symmetry at its faces.

To obtain Z_t we can induce a current in the shield by means of an exterior field coming from the outside and take the electric field on its internal surface or, by reciprocity, we can induce a current by means of a field coming from the inside and take the electric field on its exterior surface. These two ways of solving the problem are completely equivalent [12]. We have selected the second option. Therefore, we produce an incoming inner field by a longitudinal current density J_z placed along a centered inner cylinder (see fig. 2 or fig. 5).

As a boundary conditions (see fig. 2 or fig. 5), we impose on the top surface a first order absorbing boundary condition (1st ABC) adapted to

the regularized formulation [16]

$$\begin{aligned} \hat{\mathbf{n}} \times \nabla \times \mathbf{E} &= -j\omega\sqrt{\epsilon_0\mu_0}\,(\hat{\mathbf{n}} \times \hat{\mathbf{n}} \times \mathbf{E}), \\ \nabla \cdot \mathbf{E} &= -j\omega\sqrt{\epsilon_0\mu_0}\,(\hat{\mathbf{n}} \cdot \mathbf{E}), \end{aligned} \tag{6}$$

where ϵ_0 and μ_0 are, respectively, the electric permittivity and the magnetic permeability of vacuum. On the longitudinal surfaces we impose the regularized perfect magnetic conductor (PMC) condition [16]

$$\begin{aligned} \hat{\mathbf{n}} \times \nabla \times \mathbf{E} &= 0, \\ \hat{\mathbf{n}} \cdot \mathbf{E} &= 0. \end{aligned} \tag{7}$$

Finally, on the transversal surfaces we impose the regularized perfect electric conductor (PEC) condition [16]

$$\begin{aligned} \nabla \cdot (\varepsilon \mathbf{E}) &= 0, \\ \hat{\mathbf{n}} \times \mathbf{E} &= 0. \end{aligned} \tag{8}$$

The application of these boundary conditions is possible thanks to the peculiar symmetry of the electric field in the perforated tubes geometries. The PEC condition indicates that the field is normal to the transversal surfaces and the PMC condition represents that the field is parallel to the longitudinal surfaces. The expressions (6), (7) and (8) guarantee that the regularized problem (5) is well-posed, as it is demonstrated in [16].

On the other hand, the conditions (7) and (8) are not longer applicable when modeling braided wires geometries. In that case we must use periodic boundary conditions. Also, the minimum portion of geometry necessary to compute the transfer impedance is different. This portion must have the capacity to generate the whole braided wire geometry after applying successive translation symmetries in the transversal surfaces and successive rotation symmetries in the longitudinal faces of the problem domain. This model will be the topic of future work.

Summarizing, in the case of perforated tubes shields, we are solving the problem of finding $\mathbf{E} \in \mathbf{H}_0\,(\mathbf{curl}, \mathrm{div}; \Omega)$ such that, $\forall\, \mathbf{F} \in \mathbf{H}_0\,(\mathbf{curl}, \mathrm{div}; \Omega)$ holds

$$\begin{aligned} &\int_\Omega \frac{1}{\mu}\,(\nabla \times \mathbf{E}) \cdot (\nabla \times \bar{\mathbf{F}}) \\ &+ \int_\Omega \frac{1}{\mu\varepsilon\bar{\varepsilon}}\,(\nabla \cdot (\varepsilon\mathbf{E})) \cdot (\nabla \cdot (\bar{\varepsilon}\bar{\mathbf{F}})) - \omega^2 \int_\Omega \varepsilon\,(\mathbf{E} \cdot \bar{\mathbf{F}}) \\ &+ j\omega\sqrt{\frac{\epsilon_0}{\mu_0}} \int_{\partial\Omega_r} (\mathbf{E} \cdot \bar{\mathbf{F}}) = -j\omega \int_\Omega \mathbf{J} \cdot \bar{\mathbf{F}}, \end{aligned} \tag{9}$$

being $\partial\Omega_r$ the surface where the 1st ABC condition has been applied and $\mathbf{H}_0(\mathbf{curl}, \mathrm{div}; \Omega)$ the functional space defined by

$$\begin{aligned} &\mathbf{H}_0\left(\mathbf{curl}, \mathrm{div}; \Omega\right) := \\ &\quad \{\mathbf{F} \in \mathbf{H}\left(\mathbf{curl}, \mathrm{div}; \Omega\right) \mid \hat{\mathbf{n}} \times \mathbf{F} = 0 \text{ in PEC}, \\ &\qquad\qquad \hat{\mathbf{n}} \cdot \mathbf{F} = 0 \text{ in PMC}\,\}. \end{aligned} \tag{10}$$

To find the numerical solution of this problem we employed ERMES, the in-house finite element code mentioned in the previous subsection.

Once $\mathbf{E}$ is known, we must return to the equations (2) and (3) to obtain Z_t. The integration surfaces S_e and S_i are shown in fig. 6. S_e is the surface just above the shield and also includes the holes. S_i can be the forward or the backward surface in fig. 6. A third option to calculate (3) consists in doing the integration over the forward and over the backward transversal surfaces and then perform the geometric average between these two values. We must recall that the surface S_i shown in fig. 6 is only a fraction of the whole transversal section of the shield. Therefore, to calculate the total intensity flowing through the shield, which is the magnitude required in (1), we must multiply (3) by the number of times required to recover the whole transversal section. For instance, in the case shown in fig. 6, which represents a sixteenth of the whole geometry of fig. 3, we have to multiply (3) by sixteen. On the other hand, the integral (2) does not need such a multiplication. Performing the integral (2) over the surface S_e of fig. 6 give us the same result as if we performed the integral over the whole outer surface of the shield.

4 Validation

In this section we apply our numerical model to some cable shield configurations: a homogeneous tube, four different perforated tubes with circular holes and to a standard RG 58 coaxial cable tinned. As mentioned in the introduction of this paper, we have selected these configurations because they present less uncertainties than the usual configurations based on braided wires. It is left for a future work the application of the present numerical model to the study of the transfer impedance of braided wires shields.

To find the numerical solution of the problems shown here we employed the C++ code called ERMES. This code implements the finite element formulation described in the previous section. We used isoparametric tetrahedral second order nodal elements and the resulting linear system was solved

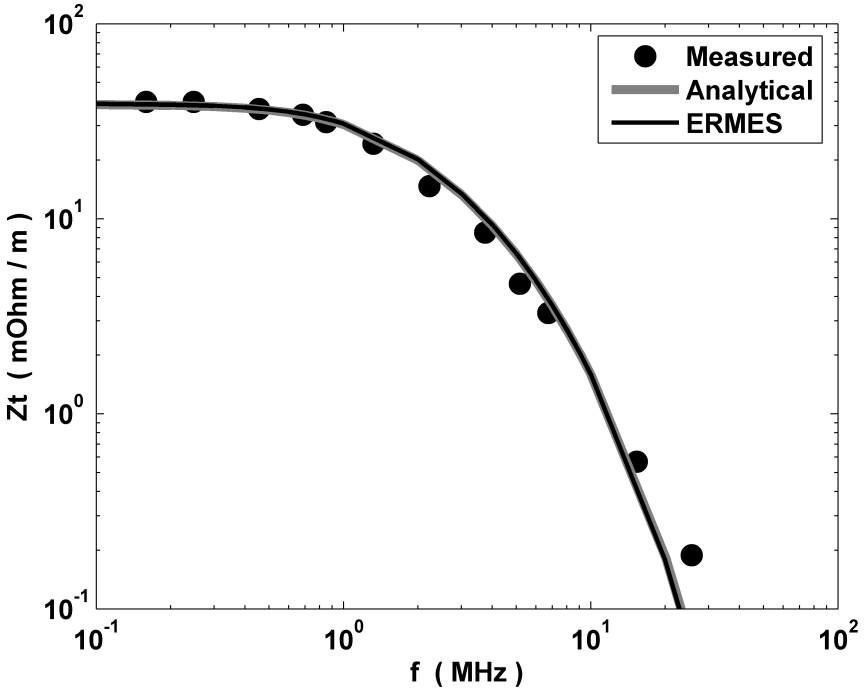

Figure 7: Transfer impedance of a stainless steal tube with an internal radius $r_{int} = 3.625\,\mathrm{mm}$, wall thickness $T = 0.91\,\mathrm{mm}$ and electrical conductivity $\sigma = 1.1e6\,\mathrm{S/m}$. Analytical results from [30]. Measurements from [31].

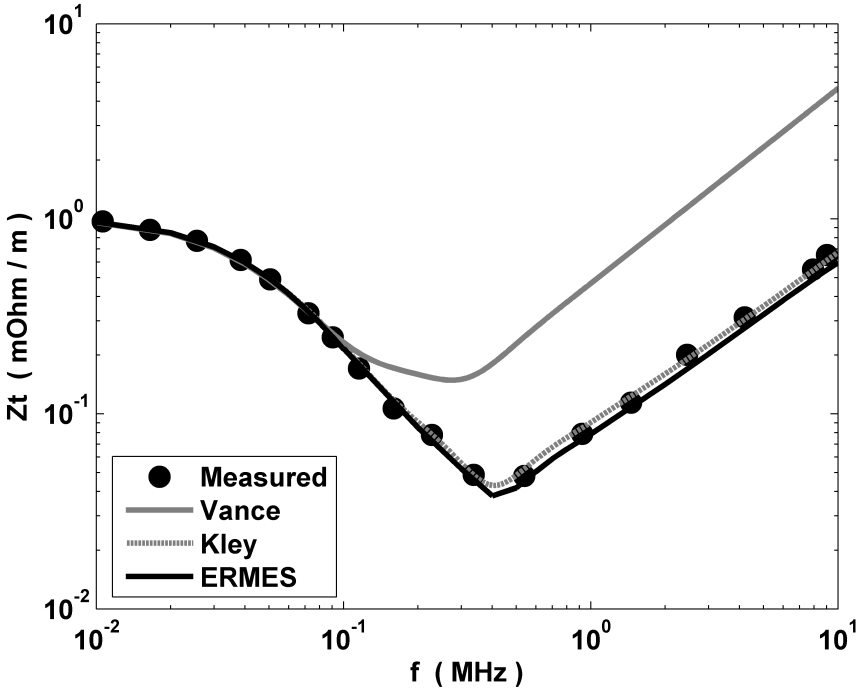

Figure 8: Transfer impedance of the perforated tube shown in fig. 1 ($\upsilon = 22\,\text{holes/meter}$, $d_h = 3.175\,\text{mm}$, $D_{ext} = 15.875\,\text{mm}$, $T = 1.683\,\text{mm}$ and $\sigma = 13.32e6\,\text{S/m}$). Analytical results from Vance [30] and Kley [7]. Measurements from [32].

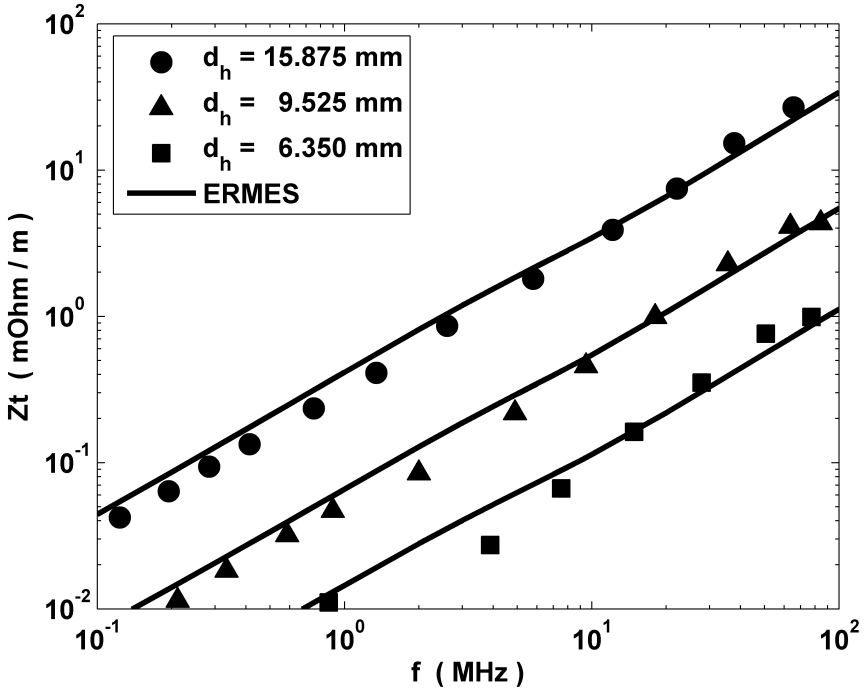

Figure 9: Transfer impedance of three copper tubes with 1 circular hole per meter. The diameter of the hole in each tube is, respectively, $d_h = 15.875\,\text{mm}$, $d_h = 9.525\,\text{mm}$ and $d_h = 6.350\,\text{mm}$. All three tubes have the same external diameter $D_{ext} = 31.750\,\text{mm}$ and the same wall thickness $T = 1.504\,\text{mm}$. It is considered an electrical conductivity for copper of $\sigma = 58e6\,\text{S/m}$ [14]. Measurements (•, ▲, ■) from [32].

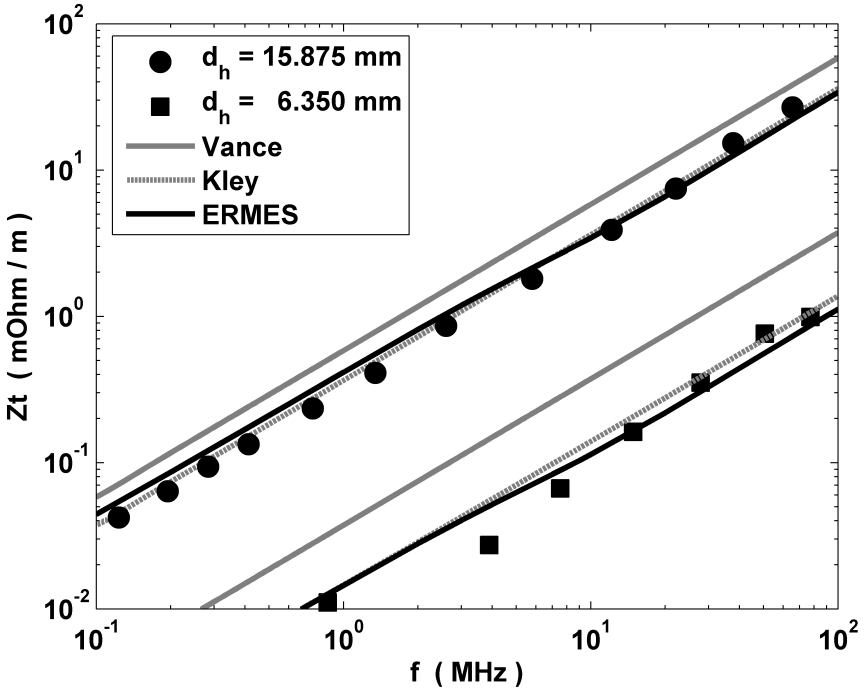

Figure 10: Transfer impedance of two of the three copper tubes shown in fig. 9. The two tubes selected are those with the maximum and the minimum hole diameter ($d_h = 15.875\,\mathrm{mm}$ and $d_h = 6.350\,\mathrm{mm}$). Analytical results from Vance [30] and Kley [7]. Measurements (•, ■) from [32].

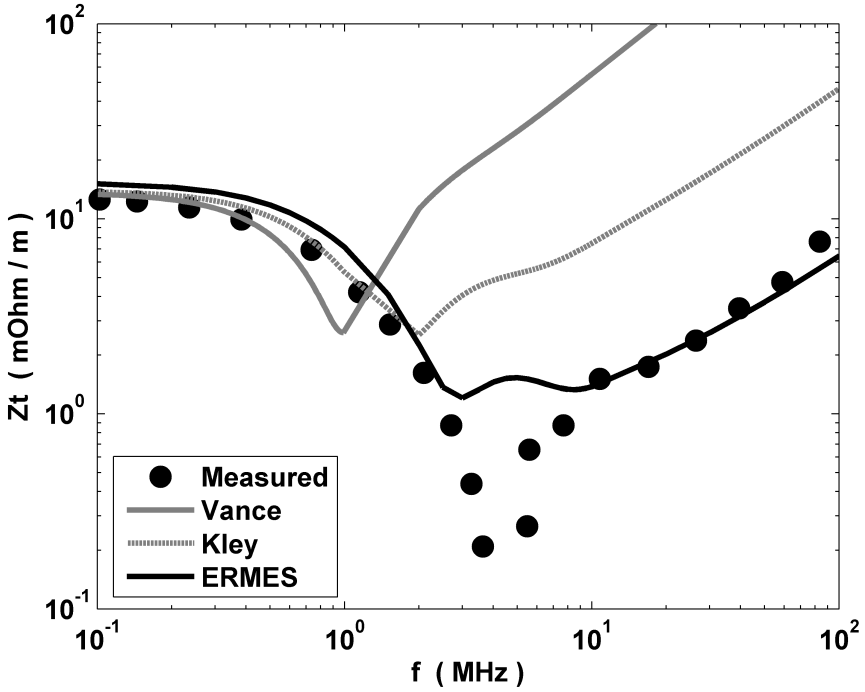

Figure 11: Transfer impedance of the shield of a standard RG 58 coaxial cable tinned. This cable shield was modeled as the perforated tube shown in fig. 3 ($D_{ext} = 3.5\,\mathrm{mm}$, $d = 0.12\,\mathrm{mm}$, $T = 2d$, $\theta = 32.32^{\mathrm{o}}$, $C = 16$, $N = 7$ and $\sigma = 32.4e6\,\mathrm{S/m}$). Analytical results from Vance [3] and Kley [7]. Measurements from [13].

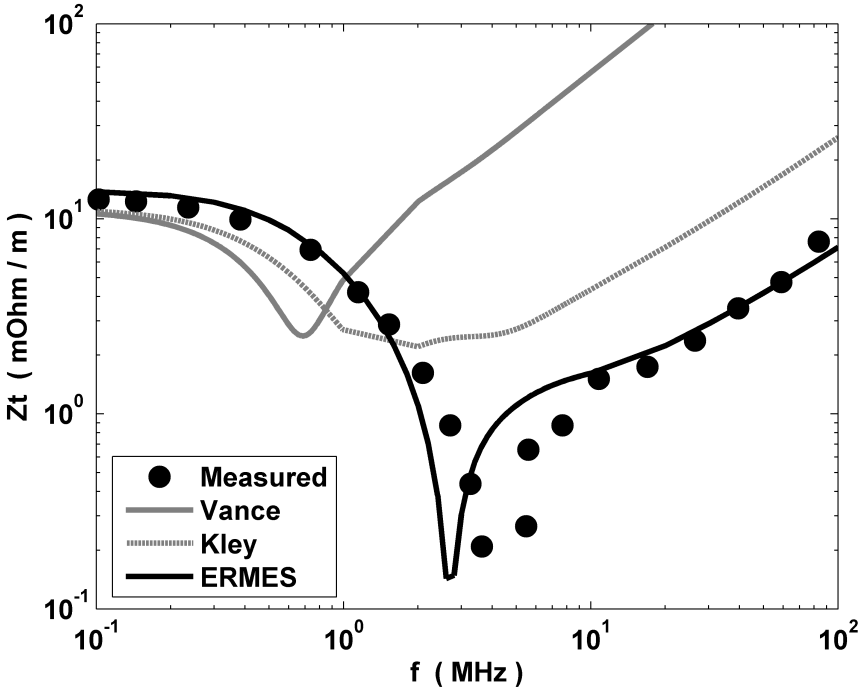

Figure 12: Transfer impedance of the shield of a standard RG 58 coaxial cable tinned. For the analytical computations with the formulas of Vance [3] and Kley [7] the shield was modeled as the perforated tube shown in fig. 3, but with the values: $D_{ext} = 3.5\,\mathrm{mm}$, $d = 0.12\,\mathrm{mm}$, $T = 2.5d$, $\theta = 32.32^{\mathrm{o}}$, $C = 16$, $N = 7$ and $\sigma = 32.4e6\,\mathrm{S/m}$. For the simulations with ERMES the shield was modeled as it is shown in fig. 4. Measurements from [13].

using a quasi-minimal residual (QMR) iterative solver [33] with a diagonal preconditioner. In all the simulations performed the convergence of the solver was excellent, proving the well-conditioning of the matrix. In average, it were used around 200000 tetrahedral second order nodal elements which produced a linear system with about 600000 unknowns. Around 700 iterations of the solver were necessary to reach a residual ($\|Ax - b\| / \|b\|$) of less than 1e-4. The memory employed was approximately 1 GB and the time spent solving each frequency was around 400 seconds. These data are referred to a desktop computer with a CPU Intel Core 2 Quad Q9300 at 2.5 GHz and the operative system Microsoft Windows XP.

4.1 Homogeneous tube

In fig. 7 is shown the transfer impedance calculated with ERMES for a stainless steal tube with an internal radius $r_{int} = 3.625\,\mathrm{mm}$, wall thickness $T = 0.91\,\mathrm{mm}$ and electrical conductivity $\sigma = 1.1e6\,\mathrm{S/m}$.

For a homogeneous tube only current diffusion is important and the values of Z_t are due to DC resistance modified by skin-effect screening. In this case, an analytical solution can be obtained from the formula given in [30]

$$Z_t = \frac{\gamma}{\sigma 2\pi a}\left(\frac{1}{sinh\,(\gamma\, T)}\right), \tag{11}$$

where $\gamma = j\omega\sqrt{\mu\,(\epsilon - j\sigma/\omega)}$ is the propagation constant in the shield material, σ is the conductivity of the shield, T is its thickness and a is its mean radius ($a = r_{int} + T/2$). The analytical results were computed using $a = 4.08\,\mathrm{mm}$, $T = 0.91\,\mathrm{mm}$ and $\sigma = 1.1e6\,\mathrm{S/m}$.

The measurements shown in fig. 7 were performed in [31]. The shield configuration consisted in the core (inner conductor plus dielectric) of a URM 67 cable with a solid stainless steel outer conductor 0.91 mm thick. In [31] is assumed an electrical conductivity of $0.8e6\,\mathrm{S/m}$ for stainless steel at room temperature. This figure is too low compared to the values found in the literature (see for instance [14] or [34]). We adopted the more reasonable value of $\sigma = 1.1e6\,\mathrm{S/m}$ for the simulations and the analytical calculations. Using $\sigma = 0.8e6\,\mathrm{S/m}$ gives the same Z_t with ERMES and (11) but the graphs are displaced upwards to respect the measurements in [31]. The numerical results of fig. 7 were obtained considering vacuum in the core of the tube. Nonetheless, simulations performed with ERMES adding a dialectic (polyethylene, $\epsilon_r = 2.3$) produced the same values of Z_t that the ones shown in fig. 7.

4.2 Perforated tubes with circular holes

Four different configurations of perforated tubes were simulated with ERMES. The first one, shown in fig. 1, has 22 circular holes per meter, each hole with a diameter $d_h = 3.175\,\mathrm{mm}$. The external diameter of the tube is $D_{ext} = 15.875\,\mathrm{mm}$ and the thickness of the wall is $T = 1.683\,\mathrm{mm}$. The tube is made of brass with an electrical conductivity of $\sigma = 13.32e6\,\mathrm{S/m}$. The results of the simulations with ERMES compared with measurements and analytical formulas are shown in fig. 8. The rest of the configurations consisted in three different copper tubes with one circular hole per meter. The diameter of the hole in each tube was, respectively, $d_h = 15.875\,\mathrm{mm}$, $d_h = 9.525\,\mathrm{mm}$ and $d_h = 6.350\,\mathrm{mm}$. All three tubes had the same external diameter $D_{ext} = 31.750\,\mathrm{mm}$ and the same wall thickness $T = 1.504\,\mathrm{mm}$. It was considered an electrical conductivity for copper of $\sigma = 58e6\,\mathrm{S/m}$. In fig. 9 are compared the results of the simulations with measurements and in fig. 10 the simulations and the measurements are compared with two different analytical approaches.

The analytical results from Vance [30] were obtained using the formula

$$Z_t = \frac{\gamma}{\sigma 2\pi a\,(1-\tau)\,sinh\,(\gamma\,T)} + j\omega\upsilon\frac{\mu_0 m}{4\pi^2 a^2}, \tag{12}$$

where υ is the number of holes per unit length, m is the polarizability of each hole, τ is the transparency of the shield and the remainder symbols represent the same as in (11). The first term of (12) is equal to the transfer impedance of a solid shield (11) except for the scalar factor $(1-\tau)$, which represents the shield coverage. For a perforated shield containing υ uniformly distributed circular holes, each with a radius r_h, we have

$$\tau = \upsilon\frac{r_h^2}{2a}. \tag{13}$$

The second term in (12) is a mutual inductance that depends on the number of openings υ in the shield and the polarizability m of each opening. For a circle of radius r_h, the polarizability is

$$m = \frac{4r_h^3}{3}. \tag{14}$$

The bad results given by (12) (see fig. 8 and fig. 10) are mainly due to the implicit assumption made in (14) that the thickness of the shield T is small compared to the radius r_h of the circular apertures. On the other hand, in the model proposed by Kley [7] the effect of a non-negligible thickness is

considered. The expression provided in [7] for the transfer impedance of a solid shield perforated with circular holes reads as follows:

$$Z_t = Z_R + \upsilon j\omega M_{LL} + \upsilon(1+j)\omega L_{SL}, \tag{15}$$

where Z_R is the transfer impedance of a solid shield, M_{LL} is the hole inductance and L_{SL} is the skin inductance. Z_R is equal to the first term of (12)

$$Z_R = \frac{\gamma}{\sigma 2\pi a\,(1-\tau)\,sinh\,(\gamma\,T)}. \tag{16}$$

M_{LL} is obtained by multiplying the inductance of a hole with negligible thickness by an attenuation factor due to the "chimney effect". The approximate formula for M_{LL} is

$$M_{LL} \approx \mu_0 \frac{0.875\,r_h^3}{3\pi^2 a^2} \exp\left(\frac{-1.84\,T}{r_h}\right). \tag{17}$$

L_{SL} models the effect of the eddy currents induced in the walls of the hole. The approximate formula for L_{SL} is

$$L_{SL} \approx \frac{T r_h}{2a^2} \exp\left(\frac{-2.30\,T}{r_h}\right) \sqrt{\frac{\mu}{2\sigma\omega}}. \tag{18}$$

The notation used in (15), (16), (17) and (18) is the same as in (12) and (11). In fig. 8 and fig. 10 is clearly observed the improvement introduced by Kley (15) respect to Vance (12).

The measurements in fig. 8, fig. 9 and fig. 10 were carried out in [32]. The data provided in [32] for the tube with $\upsilon = 22$ holes/meter (fig. 8) were only $D_{ext} = 15.875\,\text{mm}$ (5/8 in), $d_h = 3.175\,\text{mm}$ (1/8 in) and the material of the tube (brass, an alloy with an electrical conductivity between 10e6 S/m and 30e6 S/m). We deduced the thickness T and the conductivity σ from the fig. 6 in [32], where the measured transfer impedance of the same tube, but without holes, it is displayed. A $T = 1.683\,\text{mm}$ and a $\sigma = 13.32e6\,\text{S/m}$ are obtained if we solve (11) with $|Z_t|_{1\,KHz} = 1\ m\Omega/m$ and $|Z_t|_{100\,KHz} = 0.23\ m\Omega/m$. A similar situation is found for the three tubes with $\upsilon = 1$ holes/meter (fig. 9 and fig. 10). The data provided in [32] are $D_{ext} = 15.875\,\text{mm}$ (1-1/4 in), $d_h = 15.875\,\text{mm}$ (5/8 in), $d_h = 9.525\,\text{mm}$ (3/8 in), $d_h = 6.350\,\text{mm}$ (1/4 in) and the material of the tubes (copper). We accepted a conductivity for copper of $\sigma = 58e6\,\text{S/m}$ [14]. The thickness is deduced from the fig. 2 in [32], where it is shown the transfer impedance measured for the same tube but without hole. A $T = 1.504\,\text{mm}$ is obtained if we solve (11) with $|Z_t|_{1\,KHz} = 0.12\ m\Omega/m$.

4.3 Standard RG 58 coaxial cable tinned

The last validation example is the braided wire shield of a standard RG 58 coaxial cable in which the wires were fused together with a tin solder dip [13]. The braided shield consists of $C = 16$ interwoven carriers, each carrier having $N = 7$ copper wires with a diameter $d = 0.12\,\text{mm}$. The diameter of the shield is $D = 3.5\,\text{mm}$. The angle between the cable direction and the wires, the braid angle θ, is not provided in [13]. We derived θ by considering that, in general, the optical coverage of a RG 58 is $K = 0.95$ (95%) and its filling factor is less than 1 ($F < 1$). The definition of the filling factor F is [3]

$$F = \frac{CNd}{4\pi a cos\,(\theta)}, \tag{19}$$

where C is the number of carriers, N is the number of wires per carrier, d is the diameter of each wire, θ is the braid angle and a is the mean radius of the shield ($a = r_{int} + d$, where r_{int} is the inner radius of the shield). The filling factor F is related with the optical coverage K by means of the equation

$$K = 2F - F^2. \tag{20}$$

Imposing $K = 0.95$ and $F < 1$ in (20) gives $F = 0.7764$. If it is replaced this value of F in (19) with $C = 16$, $N = 7$, $d = 0.12\,\text{mm}$ and $a = 1.63\,\text{mm}$, it is finally obtained the braid angle $\theta = 32.32^{\text{o}}$.

The analytical results by Vance [3] shown in fig. 11 and 12 were obtained representing the diamond-shaped holes of fig. 3 as elliptical holes. The expression of Z_t in this case is similar to (12) but with

$$\tau = \upsilon \frac{w_e l_e}{8a} \tag{21}$$

and

$$m = \frac{\pi l_e^3}{24}\left(\frac{(1-e^2)\,e^2}{E(e) - (1-e^2)\,K(e)}\right), \tag{22}$$

where l_e is the major axis of the equivalent elliptical hole, w_e is the minor axis, e is the eccentricity $\left(e = \sqrt{1-(w_e/l_e)^2}\right)$ and $K(e)$ and $E(e)$ are the complete elliptic integrals of the first and the second kind, respectively, defined by

$$\begin{aligned} K(e) &= \int_0^{\frac{\pi}{2}} \frac{1}{\sqrt{1 - e^2 \sin^2(\varphi)}}\, d\varphi, \\ E(e) &= \int_0^{\frac{\pi}{2}} \sqrt{1 - e^2 \sin^2(\varphi)}\, d\varphi. \end{aligned} \tag{23}$$

Equation (22) is valid when $\theta < 45^{\circ}$. The parameters l_e, w_e and υ can be deduced from the known values F, θ, N and d thanks to the relations [3]

$$\upsilon = 4\pi a \sin(\theta)\cos(\theta)\left(\frac{F}{Nd}\right)^2, \tag{24}$$

$$l_e = \frac{(1-F)\,Nd}{F\sin(\theta)}, \tag{25}$$

$$w_e = \frac{(1-F)\,Nd}{F\cos(\theta)}. \tag{26}$$

The bad results given by the Vance in fig. 11 and fig. 12 can be attributed to same reason as in the previous examples with circular holes, the non-depreciable thickness of the shield to respect the size of the holes. Unfortunately, we had not found available in the literature any adaptation of the Kley's model (15) to perforated solid tubes with diamond-shaped holes. Hence, in fig. 11 and fig. 12, we employed (15) with $r_h = \sqrt{l_e w_e/4}$, that is, we approximate the rhomboidal holes as circular and with the same area as the equivalent elliptical hole. In this case, the bad results given by Kley's model can be attributed to a lack of a properly adaptation to the new circumstances.

To simulate with ERMES the tinned RG 58 cable we employed two different geometrical models. The first one is shown in fig. 3 and the results appear in fig. 11. We can see an excellent resemblance with measured data for the high frequencies range. If we want to improve the accuracy for all the frequencies it is necessary to refine our geometric model, as is done in fig. 4. As can be seen in fig. 12, when using a more realistic model the simulations and the measurements present a similar behavior in all the frequency range. We must recall that the determination of the electrical conductivity is an approximation (σ = 32.4e6 S/m, which is the average between the conductivity of copper and the conductivity of tin) and this makes also approximate the value of Z_t in the low and medium frequency range. On the other hand, at higher frequencies Z_t is almost independent of σ.

5 Conclusion

In this work we have presented a numerical model for the computation of the transfer impedance of cable shields. This model has been validated on some specific geometries comparing simulations with measurements. One

of the advantages of the numerical approach is its flexibility and its ability to deal with complex geometries and materials. Also, we had shown that our numerical model reproduces more accurately the high frequency behavior of the transfer impedance than the analytical approaches found in the literature.

In a future work the same numerical model presented here will be applied to a more real geometries where interwoven wires will be considered. The numerical model developed for perforated tubes only needs minor changes to be adapted to this situation. We only have to change the PEC and PMC boundary conditions by periodic boundary conditions and use a different minimum portion of the shield. The major difficulty in solving braided wires rest in the generation of a computer aided design (CAD) geometry ready to be used as input data for the finite element method. The generation of a braided wire CAD geometry is a time consuming task (more than the computing time of the transfer impedance itself), this is why we are currently developing a computer tool able to generate automatically this kind of geometry after being informed of the relevant parameters. This task is very important if we want to apply the numerical model to the wide variety of different braided wires shields available in the market or if we want to design new ones.

Acknowledgment

This work is part of the project HIRF-SE (High Intensity Radiated Fields Synthetic Environment), European Community's 7th Framework Programme FP7/2007-2013, ref.: 205294. The authors would like to thank the group METALFORM from CIMNE (especially to Roger Méndez, Roger Isanta and Oscar Fruitos) for their help in the realization of the CAD geometries used in this work.

References

[1] S. A. Schelkunoff, "The electromagnetic theory of coaxial transmission lines and cylindrical shields," *Bell System Technical Journal*, vol. 13, pp. 532–579, 1934.

[2] F. A. Benson, P. A. Cudd, and J. M. Tealby, "Leakage from coaxial cables," *IEE Proc.*, vol. 139, pp. 285–303, 1992.

[3] E. F. Vance, "Shielding effectiveness of braided-wire shields," *IEEE Trans. Electromagn. Compat.*, vol. 17, pp. 71–77, 1975.

[4] K. S. H. Lee and C. E. Baum, "Application of modal analysis to braided-shield cables," *IEEE Trans. Electromagn. Compat.*, vol. 17, pp. 159–169, 1975.

[5] M. Tyni, "The transfer impedance of coaxial cables with braided outer conductor," *Digest of the 10th International Worclaw Symposiom on EMC*, pp. 410–419, 1976.

[6] S. Sali, "An improved model for the transfer impedance calculations of braided coaxial cables," *IEEE Trans. Electromagn. Compat.*, vol. 33, pp. 139–143, 1991.

[7] T. Kley, "Optimized single-braided cable shields," *IEEE Trans. Electromagn. Compat.*, vol. 35, pp. 1–9, 1993.

[8] H. Haase and J. Nitsch, "High frequency model for the transfer impedance based on a generalized transmission-line theory," *IEEE International Symposium on EMC*, vol. 2, pp. 1242–1247, 2001.

[9] R. Otin, "Regularized Maxwell equations and nodal finite elements for electromagnetic field computations," *Electromagnetics*, vol. 30, pp. 190–204, 2010.

[10] J. Jin, *The Finite Element Method in Electromagnetics*, 2nd ed. John Wiley & Sons, 2002.

[11] M. Salazar-Palma, T. K. Sarkar, L.-E. García-Castillo, T. Roy, and A. Djordjevic, *Iterative and Self-Adaptive Finite-Elements in Electromagnetic Modeling*. Artech House Publishers, 1998.

[12] S. Celozzi, R. Araneo, and G. Lovat, *Electromagnetic Shielding*. John Wiley and Sons, Inc., 2008, ch. 8.

[13] R. Tiedemann, "Current flow in coaxial braided cable shields," *IEEE Trans. Electromagn. Compat.*, vol. 45, pp. 531–537, 2003.

[14] F. M. Tesche, M. Ianoz, and T. Karlsson, *EMC Analysis Methods and Computational Models*. John Wiley and Sons, Inc., 1997, ch. 10.

[15] P. A. Cudd, F. A. Benson, and J. E. Sitch, "Prediction of leakage from single braid screened cables," *IEE Proceedings A*, vol. 133, no. 3, pp. 144–151, 1986.

[16] C. Hazard and M. Lenoir, "On the solution of the time-harmonic scattering problems for Maxwell's equations," *SIAM Journal on Mathematical Analysis*, vol. 27, pp. 1597–1630, 1996.

[17] M. Costabel and M. Dauge, "Maxwell and Lamé eingevalues on polyhedra," *Mathematical Methods in Applied Science*, vol. 22, pp. 243–258, 1999.

[18] M. Costabel, "A coercive bilinear form for Maxwell's equations," *Journal of Mathematical Analysis and Applications*, vol. 157, no. 2, pp. 527–541, 1991.

[19] S. Lohrengel and S. Nicaise, "Singularities and density problems for composite materials in electromagnetism," *Communications in Partial Differential Equations*, vol. 27, no. 7, pp. 1575–1623, 2002.

[20] J. V. Bladel, *Singular Electromagnetic Fields and Sources*. IEEE Press, 1991.

[21] M. Costabel and M. Dauge, "Weighted regularization of Maxwell equations in polyhedral domains," *Numerische Mathematik*, vol. 93, no. 2, pp. 239–277, 2002.

[22] K. Preis, O. Bíró, and I. Ticar, "Gauged current vector potential and reetrant corners in the FEM analysis of 3D eddy currents," *IEEE Trans. Magn.*, vol. 36, pp. 840–843, 2000.

[23] M. Kaltenbacher and S. Reitzinger, "Appropiate finite-element formulation for 3-D electromagnetic-field problems," *IEEE Trans. Magn.*, vol. 38, pp. 513–516, 2002.

[24] K. D. Paulsen, D. R. Lynch, and J. W. Strohbehn, "Three-dimensional finite, boundary, and hybrid element solutions of the Maxwell equations for lossy dielectric media," *IEEE Trans. Microw. Theory Tech.*, vol. 36, pp. 682–693, 1988.

[25] R. Otin, "A high-order nodal finite element formulation for microwave engineering," *The 24th International Review of Progress in Applied Computational Electromagnetics (ACES 2008), March 30-April 4, Niagara Falls (Canada)*, 2008.

[26] ——, "ERMES: Numerical tool for SAR computations," International Center for Numerical Methods in Engineering (CIMNE), ref.: IT-584, Tech. Rep., 2009.

[27] ——, "Numerical study of the thermal effects induced by a RFID antenna in vials of blood plasma," International Center for Numerical Methods in Engineering (CIMNE), ref.: IT-583, Tech. Rep., 2009.

[28] O. Fruitos, R. Otin, R. Mendez, and J. Lluma, "Multiphysics simulation of metal sheet electromagnetic forming," *The 10th International Conference on Computational Plasticity, Fundamentals and Applications (COMPLAS X)*, Barcelona, Spain, 2-4 September 2009.

[29] *GiD, the personal pre and post processor*, International Center for Numerical Methods in Engineering (CIMNE), Barcelona, Spain, 2010. [Online]. Available: http://www.gidhome.com.

[30] E. F. Vance, "Shielding effectiveness of braided wire shields," *Interaction note 172*, pp. 1–39, 1974.

[31] M. M. Rahmann, J. E. Sitch, and F. A. Benson, "Leakage from coaxial cables," *IEE Proc.*, vol. 127, pp. 74–80, 1980.

[32] L. O. Hoeft and J. S. Hofstra, "Measured electromagnetic shielding perfomance of commonly used cables and connectors," *IEEE Trans. Electromagn. Compat.*, vol. 30, pp. 260–275, 1988.

[33] R. W. Freund and N. M. Nachtigal, "QMR: A quasi-minimal residual method for non-Hermitian linear systems," *SIAM Journal: Numerische Mathematik*, vol. 60, pp. 315–339, 1991.

[34] Euro Inox, *Stainless Steel: Table of Technical Properties*, ser. Materials and Applications Series. Euro Inox, 2007, vol. 5.